Evaluating the Retreat, Stabilization, and Regrowth of Crane Glacier against Marine Ice Cliff Process Models

C. Needell[1] and N. Holschuh[1*]

[1]Department of Geology, Amherst College, Amherst, MA, USA

[*]Corresponding author: Nicholas Holschuh (nholschuh@amherst.edu)

Key Points (must be < 140 characters):

- Calving of Crane Glacier's terminus after the collapse of the Larsen B Ice Shelf accelerated by 55% from 2002 until it arrested in 2004.
- 6.74 ± 0.03 km of the 10.05 km retreat occurred in floating ice, with cliff failure possible during the final phase assuming weak ice.
- Crane's retreat into a narrow fjord and sea-ice growth re-established buttressing stresses and reversed terminus retreat.

Abstract

The fastest projected rates of sea level rise appear in models which include "the marine ice cliff instability (MICI)," a hypothesized but mostly unobserved process defined by rapid, brittle failure of terminal ice cliffs that outpaces viscous relaxation and ice-shelf formation. Crane Glacier's response to the Larsen B Ice Shelf collapse has been invoked as evidence of MICI, but sparse data coverage of that event in space and time has hindered interpretation of the processes controlling terminus retreat. Using available remote sensing data, we deconstruct Crane's retreat, arrest, and regrowth over the last two decades. Much of Crane's terminus retreat occurred in floating, not grounded ice, but calving accelerated by at least 55% during the 2 years following ice shelf collapse, consistent with a positive geometric feedback. If calving occurred by cliff failure, maximum cliff heights would have been 111 m, only consistent with process models that incorporate damaged ice.

Plain Language Summary

The behavior of Antarctic glaciers will largely determine the pace and magnitude of future sea level rise. But the projections made by ice sheet models are uncertain, in part due to the uncertain response of Antarctica to the future loss of its floating ice shelves. It has been hypothesized that ice shelf breakup could trigger a self-sustaining mechanism of ice loss whereby ice cliffs collapse under their own weight. This idea is controversial because it has not been unambiguously observed in modern glacier systems. We show that after the loss of its ice shelf, Crane Glacier experienced a 2 year period of accelerating ice loss, consistent with a geometric instability like the one proposed. Models of ice cliff failure that assume glacier ice has pre-existing weaknesses are more consistent with the behavior we observe at Crane than models that assume pristine ice.

1 Introduction

The West Antarctic Ice Sheet (WAIS) is known to be a geometrically unstable system – thin near its modern margins but thick in the interior, where the ice sheet sits in deep marine basins (Morlighem et al., 2020). Because the flux of ice to the ocean by deformation and sliding scales non-linearly with ice thickness, forced retreat into the thick ice sheet interior triggers a positive feedback, increasing ice discharge and driving a self-sustaining mass imbalance that will proceed without further forcing (the Marine Ice Sheet Instability, or MISI; Weertman, 1974).

At present, WAIS is bounded by floating ice shelves, which play a critical role in buttressing ice stored in the continental interior (Dupont & Alley, 2005; Weertman, 1974). While ice shelf change over the early 21st century has been dominated by ocean driven melt from below, the disintegration of the Larsen B Ice Shelf (LBIS) by surface melt and ice-shelf hydrofracture has demonstrated that other modes of failure are possible (Glasser & Scambos, 2008), leading to a range of studies about calving dynamics and the future of Antarctic ice shelves in a warmer atmosphere (Bell et al., 2018; Kingslake et al., 2017; Lai et al., 2020).

Calving occurs most frequently by the concentration of longitudinal stresses in ice shelves at crevasse tips (Benn et al., 2007). Should WAIS experience widespread ice shelf break-up, thick glaciers could experience stresses at their termini that exceed the fracture toughness of ice. Such configurations lead to cliff failure, a specialized calving process controlled by differential stresses at the free surface of marine terminating ice fronts (Parizek et al., 2019). Cliff failure is thought to proceed faster than traditional calving, but the rate-limiting process is uncertain (DeConto & Pollard, 2016).

The "marine ice cliff instability (MICI)" is the idea that cliff failure, once initiated, accelerates with increasing cliff height. Like with MISI, forced retreat into the WAIS interior by fracture processes would then be self-sustaining. The inclusion of MICI into ice sheet models results in a sea level rise by 2100 equal to eight times the values predicted by models that do not include it (Bulthuis et al., 2019; DeConto & Pollard, 2016; Golledge et al., 2019). While it is not the only source of spread in ice sheet projections, MICI does represent the largest source of uncertainty (Fox-Kemper et al., 2021). As a result, there is a community desire to evaluate the likelihood of MICI and constrain its initiation thresholds, a focus of this work.

Recent models of cliff failure built from physics first principles (Bassis et al., 2021; Bassis & Walker, 2012; Clerc et al., 2019; Crawford et al., 2021; Parizek et al., 2019; Schlemm & Levermann, 2021; Ultee & Bassis, 2016) support MICI's theoretical validity, but the modes of failure and controlling parameters differ across them. Depending on the prescribed (but uncertain) material strength of ice, cliff-failure thresholds in the literature span from 60 to 540 m high cliffs (Clerc et al., 2019). Ice-sheet wide models rely heavily on process models (and

their underlying assumptions about ice strength) to justify parameterizations of ice-terminus dynamics.

There are few geological or geophysical observations capable of improving our understanding of ice cliff dynamics. The paleo-sea-level record may provide indirect evidence of MICI; during several periods in Earth's history, ice sheet models have difficulty reproducing the observed rapid sea level rise without it (Wise et al., 2016), but there is disagreement in the literature about whether MICI is required to explain historical Antarctic ice loss (Edwards et al., 2019). The Intergovernmental Panel on Climate Change (IPCC) names Crane Glacier's response to the LBIS collapse as the only potential evidence for MICI behavior in the satellite record (Oppenheimer et al., 2019). Crane Glacier has significantly influenced community thinking about MICI, with its post-LBIS-collapse ice calving rate used to constrain some parameterizations of cliff failure (DeConto & Pollard, 2016). But our knowledge of Crane Glacier's geometry and behavior following the LBIS collapse is limited by sparse geophysical data, challenging evaluation of whether MICI-style cliff failure occured.

By both identifying what we do know and what we cannot know based on available geophysical data, we can more precisely use Crane Glacier's behavior following the LBIS collapse event to refine our understanding of ice cliff failure. In this work, we evaluate Crane's retreat behavior and terminal characteristics against process models, to both identify whether or not unstable retreat by cliff failure was theoretically possible at Crane, and if so, what unknown model parameters must be for failure to occur there.

2 Observational Data at Crane Glacier

To use Crane Glacier as a tool for evaluating ice cliff models, we must do three things:

1. Infer the glacier geometry, the floatation state, and the grounding line position through time.
2. Show that fracture processes governed Crane's retreat behavior after the LBIS collapse.
3. Constrain the rates of retreat and their evolution through time.

All three of these objectives are observationally challenging. Brittle processes play out on very short timescales (from minutes to days) not captured by the recurrence interval of most satellite observations. In addition, we show here that ice penetrating radar data collected over Crane Glacier before the LBIS collapse failed to clearly capture the ice bottom geometry, leaving a poorly constrained ice thickness profile, grounding line position, and terminus height at the time of collapse. But by revisiting the question of Crane Glacier's response to the LBIS collapse 20 years later, this study benefits from (a) new marine geophysical measurements of the sea-floor morphology at the 2002 grounding line and (b) aircraft and satellite-measured surface elevation and ice velocity data that capture the glacier's retreat and advance in the decades following

collapse. These data allow us to better constrain the floatation state of the glacier terminus through time, refine estimates of retreat rates, and potentially narrow the range of thresholds (defined by current process models) that limit cliff failure.

1. **Surface Topography and Ice Velocity**

Glacier behavior before and after LBIS collapse is best characterized by altimetry and velocity time-series data (Figs. 1, 2). Surface elevation data were collected along the centerline of Crane Glacier by Pre-IceBridge and IceBridge campaigns (Blair et al., 2018; Studinger, 2014; Thomas & Studinger, 2010); these form the primary basis for our analysis. Satellite radar altimeters (including CryoSat-2) suffer from reduced vertical accuracy in the high slope regions of the peninsula (Fang Wang et al., 2015), and while satellite laser altimeters (including ICESat and ICESat-2) capture surface elevation with high spatial precision, their sampling is limited by cloud-cover, track orientation, and spacing in the region. Here, we use ICESat-2 data to calibrate photogrammetric DEM's produced from Maxar stereoimagery to extend the altimetry record through 2021.

There is uncertainty in the effective ice thickness at Crane in 2002 due to uncertainty in the firn air content (FAC) there (which reduces mass in the ice column, leading to stresses comparable to a shorter ice cliff than measured). The GSFC-FDMv1.1 model predicts ~15 m of FAC near the Crane terminus and its upstream catchment in 2002 (Medley et al., 2020; Figure S1), in contrast with the 0 m of FAC observed on the LBIS immediately before its collapse (Holland et al., 2011). The GSFC-FDMv1.1 does, however, agree with in-situ observations over the Larsen C (Ashmore et al., 2017). We present both the conservative cliff heights (observed height minus 15 m) and maximum possible cliff heights (observed height assuming no FAC).

In addition to using the altimetry record, we use MEaSUREs (Mouginot et al., 2017) and ITS_LIVE velocity data (Gardner et al., 2019) to characterize the evolving flow field of Crane Glacier. Together with ice terminal retreat rates, we use velocities to estimate Crane Glacier's calving rate post LBIS collapse.

2.2 Subglacial Topography and Floatation Criteria

Crane Glacier's bed elevation was refined by a marine geophysical survey in the Larsen B Inlet in 2006 (Rebesco et al., 2014), which captured the bed over which the Crane terminus retreated in 2004. Radar campaigns designed to capture ice-bottom elevations were flown as part of NASA's Operation IceBridge from 2009-2017, but because of the narrow fjords and complex topography of the Antarctic Peninsula, those data suffer from significant off-axis clutter, resulting in an ambiguous basal reflector and an unknown ice thickness profile. We use the stack of all available radar data, compared with the multibeam swath bathymetry, to derive a range of reasonable bed elevations for the glacier interior (Figures S2, S3).

Monitoring the grounding line position and quantifying the stress imbalance at a marine ice cliff requires knowledge of the ice thickness relative to the floatation thickness (the minimum ice thickness required to ground the ice bottom on the sea floor). With the density of ice (ρ_i= 917 kg/m^3), the density of sea water (ρ_{sw}= 1027 kg/m^3), and the sea-floor elevation relative to the sea surface (b), the ice height at floatation (h_f) can be calculated by:

$$h_f = b\left(1 - \frac{\rho_{\mathrm{sw}}}{\rho_i}\right)$$

Ultimately, we derive floatation heights from the radar data, multi-beam bathymetry, and estimates of the tidal state from sea-surface altimetry. This can be compared to the measured surface elevation to estimate the grounding line position. Variability in the bed topography across-flow affects our estimate of the grounding zone position. To account for this, we calculate the floatation thickness using a range of ocean bottom elevations, sampling +/- 100 m orthogonal to the centerline (Figure 1B).

2.3 The Imagery Record of Terminus Position and Sea Ice Cover

Due to infrequent collection of altimetry data over Crane, we use Landsat imagery to further constrain the timing of terminus retreat between 2002-2004. Landsat imagery also reveals the development of land-fast sea ice in the Crane Fjord in 2011 (Figure S4).

3 Retreat, Stabilization, and Regrowth of Crane Glacier

Remote sensing observations collected around the collapse event have been thoroughly discussed in the literature. Ice shelf terminus retreat and thinning preceded the rapid collapse of the LBIS in February to March of 2002 (Glasser & Scambos, 2008). We refine the following record found in the literature, which showed little change at Crane immediately post-collapse in 2002 (Scambos et al., 2004), followed by accelerated mass loss from 2003-2007 (Scambos et al., 2011), and a slow deceleration of ice loss from 2008-2013 (Wuite et al., 2015).

The MICI hypothesis, invoked for Crane, is predicated on the idea that calving by cliff failure (and terminus retreat into thicker ice with taller cliffs) causes an acceleration of the calving rate that outpaces the ability of Crane to viscously thin and inhibit calving. Below, we reframe and extend the observational record of Crane Glacier from 2002-2021 to highlight three distinct periods with the MICI hypothesis in mind: the initiation of fracture processes and accelerating terminus retreat, the stabilization of the glacier terminus, and the regrowth and return to glacier equilibrium with the modern climate. We argue these data show the disequilibrium behavior of Crane Glacier during retreat, including a positive geometric feedback as retreat accelerates, and hysteresis in its response as it returns to an advanced but thin configuration within the modern climate.

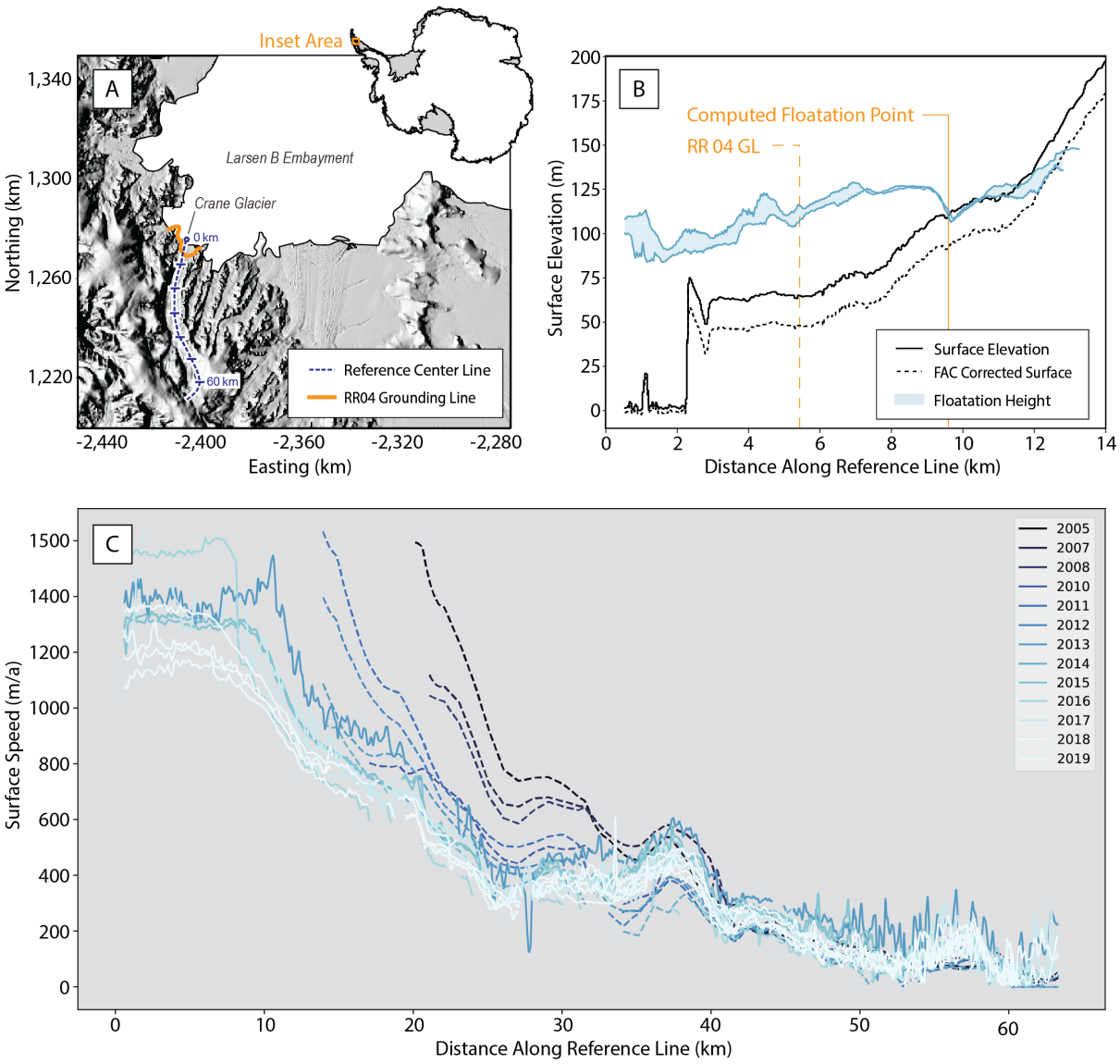

Figure 1. Crane Glacier's (a) location, (b) floatation state, and (c) ice velocity through time. (a) Hillshade map of the Larsen B Ice Shelf region, showing a reference centerline (dashed blue, annotated every 10 km, which we use for all subsequent along-flow transects) and an early, satellite-derived estimate of the 2002 grounding line (Rack & Rott, 2004; "RR04"; orange). (b) Range of floatation heights and ice surface elevations in November 2002 with our updated grounding line. (c) ITS_LIVE (solid) and MEaSUREs (dashed) ice velocity profiles along the flight line from 2005-2019.

3.1 Period 1: Retreat (2002-2004)

From 2002-2004, terminus retreat of over 10 km occurred, with moderate retreat rates from November 2002 to March 2004, and more rapid retreat from March to November 2004 (Figure 2). During this two year window, the glacier thinned by 60.9 m at the location of the November 2004 ice front.

Satellite-derived, pre-LBIS collapse grounding line positions do not agree with the sea-floor sedimentary record or the updated bathymetry measured post-collapse (Rebesco et al., 2014). Satellite data placed the pre-collapse grounding line near the opening of the fjord (Rack & Rott, 2004), implying that the full extent of retreat observed from 2002-2004 occurred by failure of a grounded ice cliff. Radiocarbon-dated sediment cores show that ice was not grounded there in 2002, and suggest the pre-collapse grounding line was located further inland of the fjord opening (Rebesco et al., 2014). In addition, measured surface elevations from 2002 at the purported grounding line fell far below the floatation threshold (Fig. 1B). This means that a substantial portion of the initial terminus retreat occurred in ice that was at or below the floatation thickness.

Using our floatation criterion, we calculate an updated grounding line position for November 2002. Surface elevation data show a break in slope at ~9.5 km along our reference line, more consistent with calculated grounding lines assuming 0 m of FAC. We calculate retreat rates and cliff heights assuming this value.

While the majority of the Larsen B collapsed during February and March of 2002, a floating ice shelf remained at Crane. Slow terminus retreat began, but had not reached the 2002 grounding line by March of 2004, after 5.30 km of retreat (Figure 2). Retreat continued, and during the following 8 month period, the glacier experienced 4.75 km of additional terminus retreat, beginning 1.47 $\pm$ 0.03 km down-flow of the updated 2002 grounding line and halting at the 2004 terminus. We quantify the effective rate of ice loss during the periods preceding and following March 26, 2004 using a calving rate, equal to the sum of the terminus retreat rate and the ice flow speed at the terminus (~1.5 km per year, the nearest available satellite measurement in space and time, and consistent with estimates from Scambos et al., 2004). This results in minimum calving rate estimates of 5.48 km/a for the period ending on March 26, 2004, and 8.50 km/a in the period after, a 55% increase in calving rate over the 2 years following LBIS collapse.

If grounded ice cliff failure occurred at Crane, it must have happened during this final period of retreat. While there are no direct observations of a grounded ice cliff during that period, the first cliff that could have formed (at the 2002 grounding line position) would have existed with a height of 111 m (as measured above the water line; Figure 1B).

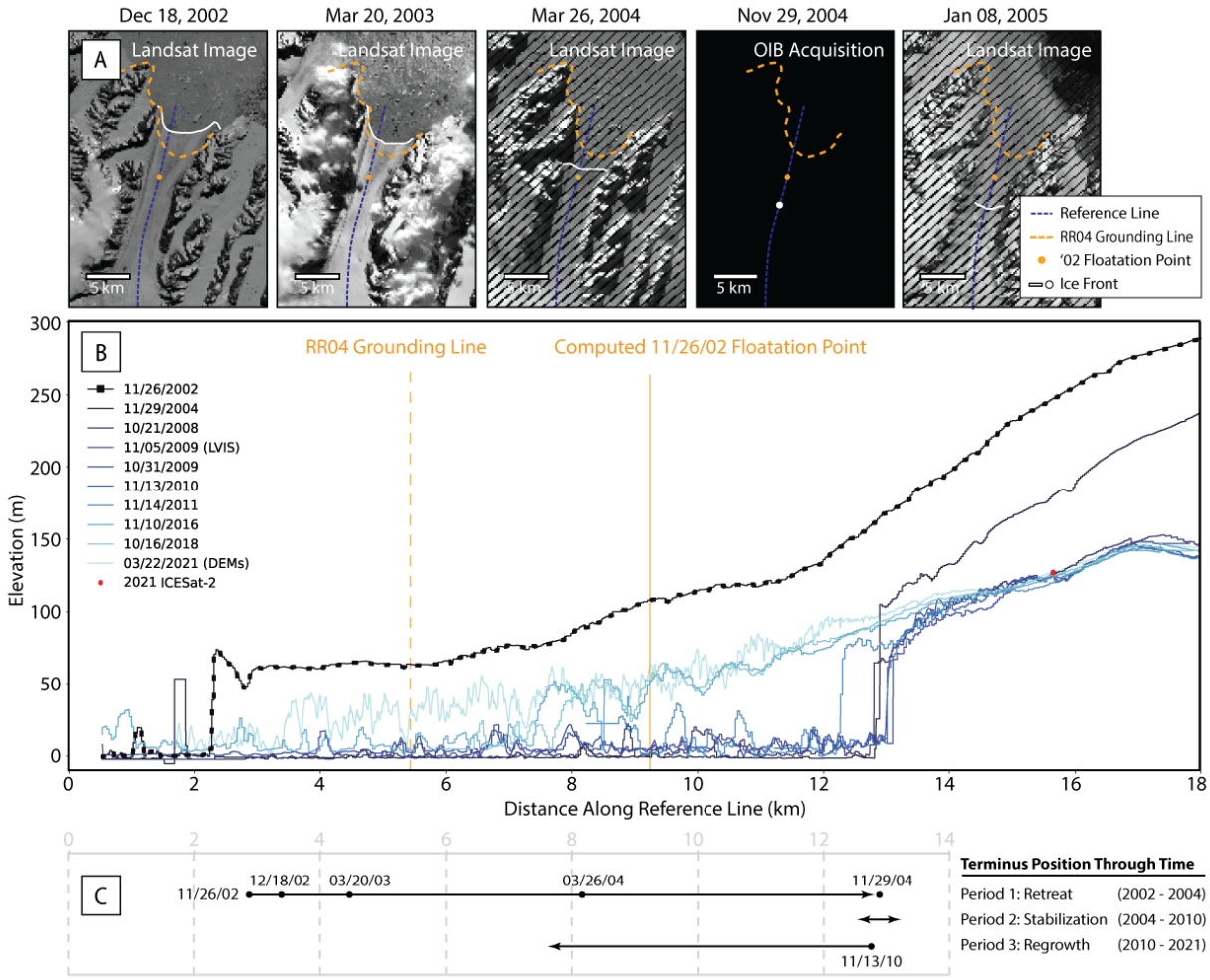

Figure 2. Data used to constrain timing of terminus retreat. (a) Landsat images of the Crane terminus, with manually-identified ice fronts (white), the Rack & Rott (2004) grounding line, and the calculated 2002 floatation point (orange) shown. (b) Altimetry record of near-terminus surface elevation, from NASA's ATM and LVIS altimeters (2002-2018), and ICESat-2-calibrated photogrammetric DEMs produced from Maxar stereoimagery (2021). (c) Terminus evolution through time, corresponding to ice fronts in (a) and altimetry in (b).

3.2 Period 2: Stabilization (November 2004-2010)

By November 2004, the terminus of Crane Glacier had ceased its retreat 10.05 km upstream of its November 2002 terminus. The terminus remained stationary for the following six years, with a terminal cliff and terminus position that fluctuated by less than 500 m during that period. One of two conditions must have

been met: either (a) the calving rate fell to the glacier speed at that location, or (b) this position defined the threshold for cliff failure, with a calving rate much higher than the ice velocity downstream and a cliff calving rate of 0 km/a upstream. Meanwhile, the system adjusted to the large mass-disequilibrium by thinning upstream (Figure S5), reducing the driving stress and slowing its flow speed. This period saw an average thickness change of -16.3 m/a (0-15 km from the terminus) and a maximum velocity change of approximately -237.5 m/a^2, which occurred between 2005-2007 (0-20 km from the terminus).

3.3 Period 3: Regrowth (2010-2021)

From 2010-present, Crane's terminus has advanced and slowed. From 2010-2011, the terminus advanced by 0.45 km. Limited elevation data were collected along Crane's flowline between 2012-2015, but surface elevation data from 2016-2018 capture an active calving front. This new terminus position sits approximately 1.25 km downstream of the 2010 terminus. Crane Glacier's near-terminus surface elevation increased by approximately 5 m/a over this 11 year period, as captured by ICESat-2 calibrated photogrammetric DEMs from 2019-2021 (Figures 2, S5). This thickening represents a redistribution of mass from the tributaries, where thinning of approximately 5 m/year occurred from 2019-2021, to the trunk (Figure S5).

4 Discussion

4.1 Evaluating the Retreat Behavior of Crane Glacier

Without observations during the rapid 8 month retreat window, there is no direct evidence of ice cliff failure at Crane Glacier. But there is evidence for a geometric instability in the system, and indirect evidence that cliff failure may have occurred. We examine these two ideas separately.

As we observed at Crane, fracture processes dominated following LBIS breakup, where a terminal ice cliff was observed from 2002-2004. But immediately following the forcing event (LBIS collapse), retreat by fracture was slow. As the terminus retreated into thicker ice, calving and retreat rates increased despite no new climatic forcing, consistent with a geometric instability. Retreat continued, with a rapid final phase occurring where the ice had been clearly grounded in 2002. The system eventually reached a configuration with a terminal stress state that inhibited further retreat, and the system restabilized.

Many conditions are known to inhibit cliff failure and stabilize glacier systems, including narrowing of the fjord (Schlemm & Levermann, 2021), development of sea-ice or mélange in the fjord which can apply sufficient backstress to stabilize the cliff (Bassis et al., 2021; Crawford et al., 2021; Schlemm & Levermann, 2021), retreat into thinner ice along a prograde slope (Bassis et al., 2021), or retreat into ice that is not preconditioned for failure by crevassing or other processes that induce damage (Clerc et al., 2019). As Crane's terminus retreated, the fjord narrowed to a point where calving and ice flow were in balance. Then, viscous processes dominated, and the system thinned. In summer 2011, peren-

nial land-fast sea ice formed in Crane Glacier's embayment (Figure S4), which likely enabled the growth of an ice shelf, consistent with models of sea ice backstress (Robel, 2017) and documented sea-ice circulation patterns in the region (Christie et al., 2022). The reestablishment of a floating ice shelf facilitated Crane Glacier's recent thickening and velocity decrease.

Cliff failure is thought to be one of the fastest calving processes. Crane's final minimum calving rate of 8.50 km/a represented an increase of both its pre-collapse ice shelf calving rate (Alley et al., 2008) and its calving rate during the initial period following collapse, which could indicate a change in the mechanism of calving over that period. But rates greater than 11 km/a have been recently observed elsewhere on the WAIS (Milillo et al., 2022), and at Jakobshavn and Helheim Glaciers in Greenland, whose calving rates exceed 17 km/a (Joughin et al., 2014) and 11 km/a (Howat et al., 2005), respectively. The calving rates at Jakobshavn and Helheim, in part, accommodate their high terminus velocities (9.5 to 15.5 km/a faster than the terminus of Crane), which is an important qualitative difference between these systems and Crane. As such, the calving rate observed at Crane does not fall outside of the range experienced by floating systems elsewhere in Antarctica and Greenland, but is anamolous for a glacier flowing only 1.5 km/a at its terminus.

Ultimately, we see 10.05 km of terminus retreat, 3.28 ± 0.03 km of which could have occurred in grounded ice, with calving rates that accelerated over the course of retreat.

4.2 Evaluating Crane Retreat against Process Models

Models of ice cliff failure each have a stability threshold, defining the boundary between configurations that naturally fail and those in which cliffs are stable and glaciers will thin and evolve by viscous processes. We evaluate the behavior of Crane against published ice cliff process models (Bassis et al., 2021; Bassis & Ultee, 2019; Bassis & Walker, 2012; Clerc et al., 2019; Crawford et al., 2021; Parizek et al., 2019; Ultee & Bassis, 2016).

A number of mechanisms exist under the "cliff failure" umbrella, including: fracture-induced full-thickness iceberg detachment (Bassis et al., 2021); initial slumping followed by buoyancy-driven retrogressive block rotation (Parizek et al., 2019; Bassis et al., 2021; Crawford et al., 2021); and forward block rotation resulting from surface crevassing (Crawford et al., 2021). Each model is built from a different physical framework, and therefore requires as input a different quantification of the material strength of ice. Ice strength appears in models through terms like the fracture toughness (Clerc et al., 2019; Crawford et al., 2021; Parizek et al., 2019), the yield strength (Bassis et al., 2021; Bassis & Ultee, 2019; Crawford et al., 2021; Ultee & Bassis, 2016), or critical strain thresholds (Crawford et al., 2021). Ideally, these terms can be constrained by laboratory measurements using physics first-prinicples (Druez et al., 1989; Petrovic, 2003; Xian et al., 1989), but in practice, they remain uncertain, as they are affected by the uncertain history of ice damage that modifies real glacier systems (Borstad

et al., 2012; Lhermitte et al., 2020; Mobasher et al., 2016).

Because of this parametric uncertainty, the models we compare against observations at Crane produce a range of possible cliff-failure thresholds, assuming strength values ranging from intact or undamaged ice (strong) to ice with a lower yield strength (Ultee & Bassis, 2016), lower fracture toughness (Clerc et al. 2019; Parizek et al. 2019), or ice including starter cracks (Bassis et al., 2021) (weak). We proceed using each model's self-described optimum parameters, but present alternative "strong" or "weak" failure thresholds in Figure 3 if available (see the Supplementary Materials for a full description of model thresholds and strength categorization).

Using nominal (strong) ice, process models require greater cliff heights (Bassis & Ultee, 2019; Bassis & Walker, 2012; Clerc et al., 2019; Crawford et al., 2021; Parizek et al., 2019; Ultee & Bassis, 2016) and faster timescales of ice shelf collapse (Clerc et al., 2019) than we observe at Crane Glacier to initiate retreat by cliff failure (Figure 3). When ice is treated as weak or damaged, process models predict that cliff failure could initiate at Crane with a terminus height of 111 m. This suggests that it is possible for accelerated calving to have occurred by cliff failure, and if so, models might more accurately predict MICI initiation if they consider weak ice a realistic scenario, rather than an extreme one.

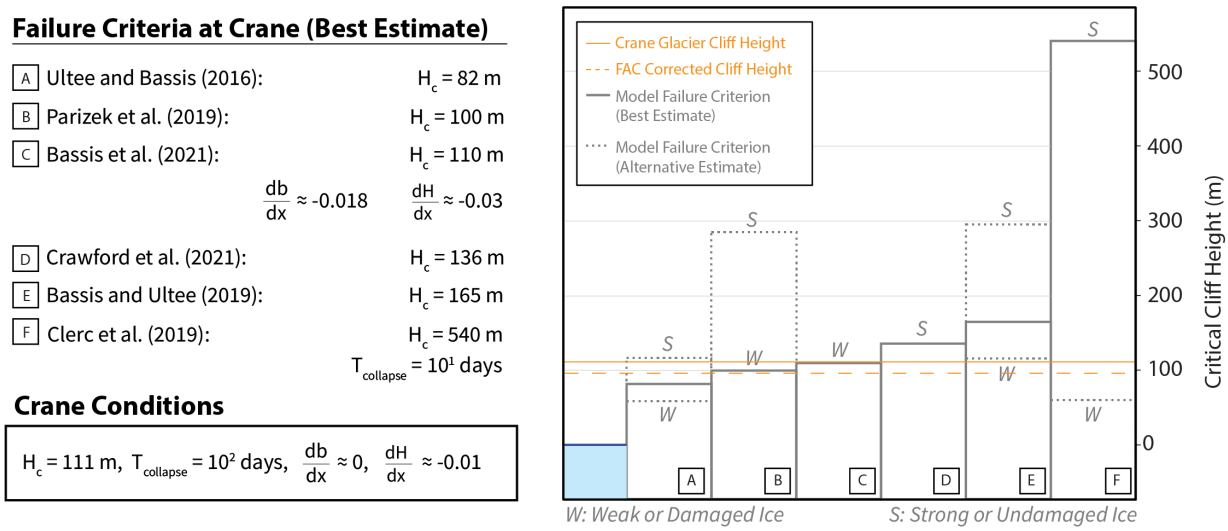

Figure 3. Conditions at Crane Glacier compared to process model cliff-failure thresholds. (Left) Cliff-height failure criteria required to trigger MICI (see Text S1; Figure S6, S7), including subaerial cliff height (H_c), bed slope ($\frac{db}{dx}$), ice thickness gradient ($\frac{dH}{dx}$), and timescale of ice shelf collapse ($T_{collapse}$), with conditions we observe at Crane Glacier provided. (Right) Schematic diagram comparing cliff heights required for brittle failure under strong (S) and weak (W) model treatment of ice, if included in referenced work (with the model authors'

preferred estimate marked with a solid line).

5 Conclusions

Despite Crane Glacier being invoked in many conversations of unstable ice cliff failure, the limited data collected during the LBIS collapse never directly measured a cliff failure event. Previous analysis of Crane Glacier's behavior from 2002-2004 is predicated on an inaccurate 2002 grounding line position. Our analysis shows that retreat in 2002 and 2003 occurred in a remnant, floating ice shelf, but in the two years following LBIS collapse, calving rates accelerated, consistent with a positive feedback and geometric instability. This includes the final phase of retreat, which may have occurred by the failure of a grounded ice cliff with an initial height of 111 m, with a minimum calving rate of ~8.50 km/a.

The glacier terminus retreated to a configuration where calving rates slowed, and the system maintained a constant terminus position for 7 years with no further retreat. Meanwhile, the mass dis-equilibrium induced by terminus changes drove widespread thinning in the glacier interior. Finally, as sea-ice filled the fjord in 2011, Crane Glacier's terminus advanced and an ice shelf was re-established, supporting a thickening and slowing (but overall thinner than pre-LBIS collapse) glacier profile.

Given a maximum terminal cliff height of only 111 m, available process models indicate that terminus stresses would not exceed the failure threshold of undamaged ice. However, using model values consistent with damaged ice, cliff failure at Crane Glacier becomes consistent with the process models discussed here. This highlights the importance of better understanding ice shelf damage in projecting future ice sheet behavior – if high damage is plausible for Crane Glacier, it means that cliff failure likely did govern the final stage of glacier retreat, and future ice sheet margins may be more susceptible to fracture than anticipated.

The rapid nature of ice shelf break-up makes observing ice cliff failure an inherently challenging problem. Brittle processes are fast and therefore require high temporal sampling to observe, best accomplished in situ. Measuring cliff failure processes will require having field sensors in the right place at the right time, something not easily done at scale. This means that observational evaluation of ice cliff models must, in part, rely on the temporally limited (and therefore at times, ambiguous) remote sensing record. While studies like this one cannot end the debate over model realism and the role of cliff failure in the future evolution of the Antarctic Ice Sheet, they contribute to the larger corpus of evidence required to justify any novel treatment of cliffs in continental scale models of Antarctica and Greenland.

Acknowledgments

This work was funded through NASA award 80NSSC20K0958. We would like to thank the Polar Geospatial Center, who provided stereo-pair DEMs gener-

ated from MAXAR imagery over Crane Glacier. We would also like to thank Lizz Ultee and our other anonymous reviewer for their useful and constructive feedback, which ultimately led to a much stronger manuscript.

Data Availability Statement

Data compiled for figures 1 and 2 of this manuscript are provided through Harvard Dataverse: https://doi.org/10.7910/DVN/SOFZR7. Pre-IceBridge and IceBridge altimetry data, and MEaSUREs velocity data were downloaded from the National Snow and Ice Data Center at: https://nsidc.org/data/BLATM2/versions/1, https://nsidc.org/data/ILATM2/versions/2, and https://nsidc.org/data/NSIDC-0720/versions/1. Velocity data generated using autoRIFT (Gardner et al., 2018) and provided by the NASA MEaSUREs ITS_LIVE project (Gardner et al., 2019) were downloaded from the following repository: https://github.com/nasa-jpl/its_live. Landsat images were downloaded from https://earthexplorer.usgs.gov. Figures were made with Matplotlib version 3.4.3, available under the Matplotlib license at https://matplotlib.org/.

References

Alley, R. B., Horgan, H. J., Joughin, I., Cuffey, K. M., Dupont, T. K., Parizek, B. R., Anandakrishnan, S., & Bassis, J. (2008). A Simple Law for Ice-Shelf Calving. *Science*, *322*(5906), 1344–1344. https://doi.org/10.1126/science.1162543Ashmore, D. W., Hubbard, B., Luckman, A., Kulessa, B., Bevan, S., Booth, A., Munneke, P. K., O'Leary, M., Sevestre, H., & Holland, P. R. (2017). Ice and firn heterogeneity within Larsen C Ice Shelf from borehole optical televiewing. *Journal of Geophysical Research: Earth Surface*, *122*(5), 1139–1153. https://doi.org/10.1002/2016JF004047Bassis, J. N., Berg, B., Crawford, A. J., & Benn, D. I. (2021). Transition to marine ice cliff instability controlled by ice thickness gradients and velocity. *Science*, *372*(6548), 1342–1344. https://doi.org/10.1126/science.abf6271Bassis, J. N., & Ultee, L. (2019). A Thin Film Viscoplastic Theory for Calving Glaciers: Toward a Bound on the Calving Rate of Glaciers. *Journal of Geophysical Research: Earth Surface*, *124*(8), 2036–2055. https://doi.org/10.1029/2019JF005160Bassis, J. N., & Walker, C. C. (2012). Upper and lower limits on the stability of calving glaciers from the yield strength envelope of ice. *Proceedings of the Royal Society A: Mathematical, Physical and Engineering Sciences*, *468*(2140), 913–931. https://doi.org/10.1098/rspa.2011.0422Bell, R. E., Banwell, A. F., Trusel, L. D., & Kingslake, J. (2018). Antarctic surface hydrology and impacts on ice-sheet mass balance. *Nature Climate Change*, *8*(12), 1044–1052. https://doi.org/10.1038/s41558-018-0326-3Benn, D. I., Warren, C. R., & Mottram, R. H. (2007). Calving processes and the dynamics of calving glaciers. *Earth-Science Reviews*, *82*(3–4), 143–179. https://doi.org/10.1016/j.earscirev.2007.02.002Blair, J. B., Hofton, M. A., & Rabine, D. L. (2018). *Processing of NASA LVIS elevation and canopy (LGE, LCE and LGW) data products.* http://lvis.gsfc.nasa.govBorstad, C. P., Khazendar, A., Larour, E., Morlighem, M., Rignot, E., Schodlok, M. P., & Seroussi, H. (2012). A damage mechanics assessment of the Larsen B ice shelf prior to

collapse: Toward a physically-based calving law. *Geophysical Research Letters*, *39*(18). https://doi.org/10.1029/2012GL053317Bulthuis, K., Arnst, M., Sun, S., & Pattyn, F. (2019). Uncertainty quantification of the multi-centennial response of the Antarctic ice sheet to climate change. *The Cryosphere*, *13*(4), 1349–1380. https://doi.org/10.5194/tc-13-1349-2019Christie, F. D. W., Benham, T. J., Batchelor, C. L., Rack, W., Montelli, A., & Dowdeswell, J. A. (2022). Antarctic ice-shelf advance driven by anomalous atmospheric and sea-ice circulation. *Nature Geoscience*, *15*(5), 356–362. https://doi.org/10.1038/s41561-022-00938-xClerc, F., Minchew, B. M., & Behn, M. D. (2019). Marine Ice Cliff Instability Mitigated by Slow Removal of Ice Shelves. *Geophysical Research Letters*, *46*(21), 12108–12116. https://doi.org/10.1029/2019GL084183Crawford, A. J., Benn, D. I., Todd, J., Åström, J. A., Bassis, J. N., & Zwinger, T. (2021). Marine ice-cliff instability modeling shows mixed-mode ice-cliff failure and yields calving rate parameterization. *Nature Communications*, *12*(1), 2701. https://doi.org/10.1038/s41467-021-23070-7DeConto, R. M., & Pollard, D. (2016). Contribution of Antarctica to past and future sea-level rise. *Nature*, *531*(7596), 591–597. https://doi.org/10.1038/nature17145Druez, J., McComber, P., & Tremblay, C. (1989). Experimental results on the tensile strength of atmospheric ice. *Transactions of the Canadian Society for Mechanical Engineering*, *13*(3), 59–64. https://doi.org/10.1139/tcsme-1989-0010Dupont, T. K., & Alley, R. B. (2005). Assessment of the importance of ice-shelf buttressing to ice-sheet flow. *Geophysical Research Letters*, *32*(4). https://doi.org/10.1029/2004GL022024Edwards, T. L., Brandon, M. A., Durand, G., Edwards, N. R., Golledge, N. R., Holden, P. B., Nias, I. J., Payne, A. J., Ritz, C., & Wernecke, A. (2019). Revisiting Antarctic ice loss due to marine ice-cliff instability. *Nature*, *566*(7742), 58–64. https://doi.org/10.1038/s41586-019-0901-4Fang Wang, Bamber, J. L., & Xiao Cheng. (2015). Accuracy and Performance of CryoSat-2 SARIn Mode Data Over Antarctica. *IEEE Geoscience and Remote Sensing Letters*, *12*(7), 1516–1520. https://doi.org/10.1109/LGRS.2015.2411434Fox-Kemper, B., Hewitt, H. T., Xiao, C., Aðalgeirsdóttir, G., Drijfhout, S. S., Edwards, T. L., Golledge, N. R., Hemer, M., Kopp, R. E., Krinner, G., Mix, A., Notz, D., Nowicki, S., Nurhati, I. S., Ruiz, L., Sallée, J.-B., Slangen, A. B. A., & Yu, Y. (2021). Ocean, Cryosphere and Sea Level Change. In V. Masson-Delmott, P. Zhai, A. Pirani, S. L. Connors, C. Péan, S. Berger, N. Caud, Y. Chen, L. Goldfarb, M. I. Gomis, M. Huang, K. Leitzell, E. Lonnoy, J. B. R. Matthews, T. K. Maycock, T. Waterfield, O. Yelekçi, R. Yu, & B. Zhou (Eds.), *Climate Change 2021: The Physical Science Basis. Contribution of Working Group I to the Sixth Assessment Report of the Intergovernmental Panel on Climate Change* (pp. 1211–1362). Cambridge University Press. 10.1017/9781009157896.011Gardner, A. S., Fahnestock, M. A., & Scambos, T. A. (2019). *MEaSUREs ITS_LIVE Landsat Image-Pair Glacier and Ice Sheet Surface Velocities: Version 1.* https://doi.org/10.5067/IMR9D3PEI28UGlasser, N. F., & Scambos, T. A. (2008). A structural glaciological analysis of the 2002 Larsen B ice-shelf collapse. *Journal of Glaciology*, *54*(184), 3–16. https://doi.org/10.3189/002214308784409017Golledge, N. R., Keller, E. D.,

Gomez, N., Naughten, K. A., Bernales, J., Trusel, L. D., & Edwards, T. L. (2019). Global environmental consequences of twenty-first-century ice-sheet melt. *Nature*, *566*(7742), 65–72. https://doi.org/10.1038/s41586-019-0889-9Holland, P. R., Corr, H. F. J., Pritchard, H. D., Vaughan, D. G., Arthern, R. J., Jenkins, A., & Tedesco, M. (2011). The air content of Larsen Ice Shelf. *Geophysical Research Letters*, *38*(10), n/a-n/a. https://doi.org/10.1029/2011GL047245Howat, I. M., Joughin, I., Tulaczyk, S., & Gogineni, S. (2005). Rapid retreat and acceleration of Helheim Glacier, east Greenland. *Geophysical Research Letters*, *32*(22). https://doi.org/10.1029/2005GL024737Joughin, I., Smith, B. E., Shean, D. E., & Floricioiu, D. (2014). Brief Communication: Further summer speedup of Jakobshavn Isbræ. *The Cryosphere*, *8*(1), 209–214. https://doi.org/10.5194/tc-8-209-2014Kingslake, J., Ely, J. C., Das, I., & Bell, R. E. (2017). Widespread movement of meltwater onto and across Antarctic ice shelves. *Nature*, *544*(7650), 349–352. https://doi.org/10.1038/nature22049Lai, C.-Y., Kingslake, J., Wearing, M. G., Chen, P.-H. C., Gentine, P., Li, H., Spergel, J. J., & van Wessem, J. M. (2020). Vulnerability of Antarctica's ice shelves to meltwater-driven fracture. *Nature*, *584*(7822), 574–578. https://doi.org/10.1038/s41586-020-2627-8Lhermitte, S., Sun, S., Shuman, C., Wouters, B., Pattyn, F., Wuite, J., Berthier, E., & Nagler, T. (2020). Damage accelerates ice shelf instability and mass loss in Amundsen Sea Embayment. *Proceedings of the National Academy of Sciences*, *117*(40), 24735–24741. https://doi.org/10.1073/pnas.1912890117Medley, B., Neumann, T. A., Zwally, H. J., & Smith, B. E. (2020). Forty-year Simulations of Firn Processes over the Greenland and Antarctic Ice Sheets. *The Cryosphere Discussions*, 1–35. https://doi.org/10.5194/tc-2020-266Milillo, P., Rignot, E., Rizzoli, P., Scheuchl, B., Mouginot, J., Bueso-Bello, J. L., Prats-Iraola, P., & Dini, L. (2022). Rapid glacier retreat rates observed in West Antarctica. *Nature Geoscience*, *15*(1), 48–53. https://doi.org/10.1038/s41561-021-00877-zMobasher, M. E., Duddu, R., Bassis, J. N., & Waisman, H. (2016). Modeling hydraulic fracture of glaciers using continuum damage mechanics. *Journal of Glaciology*, *62*(234), 794–804. https://doi.org/10.1017/jog.2016.68Morlighem, M., Rignot, E., Binder, T., Blankenship, D., Drews, R., Eagles, G., Eisen, O., Ferraccioli, F., Forsberg, R., Fretwell, P., Goel, V., Greenbaum, J. S., Gudmundsson, H., Guo, J., Helm, V., Hofstede, C., Howat, I., Humbert, A., Jokat, W., … Young, D. A. (2020). Deep glacial troughs and stabilizing ridges unveiled beneath the margins of the Antarctic ice sheet. *Nature Geoscience*, *13*(2), 132–137. https://doi.org/10.1038/s41561-019-0510-8Mouginot, J., Scheuchl, B., & Rignot, E. (2017). *MEaSUREs Annual Antarctic Ice Velocity Maps, Version 1.* NASA National Snow and Ice Data Center Distributed Active Archive Center. https://doi.org/10.5067/9T4EPQXTJYW9Oppenheimer, M., Glavovic, B. C., Hinkel, J., van de Wal, R., Magnan, A. K., Abd-Elgawad, A., Cai, R., Cifuentes-Jara, M., Rica, C., DeConto, R. M., Ghosh, T., Hay, J., Islands, C., Isla, F., Marzeion, B., Meyssignac, B., Sebesvari, Z., Biesbroek, R., Buchanan, M. K., … Pereira, J. (2019). *Sea Level Rise and Implications for Low-Lying Islands, Coasts and Communities.*Parizek, B. R., Christianson,

K., Alley, R. B., Voytenko, D., Vaňková, I., Dixon, T. H., Walker, R. T., & Holland, D. M. (2019). Ice-cliff failure via retrogressive slumping. *Geology*, *47*(5), 449–452. https://doi.org/10.1130/G45880.1Petrovic, J. J. (2003). Mechanical properties of ice and snow. *Journal of Materials Science*, *38*, 1–6.Rack, W., & Rott, H. (2004). Pattern of retreat and disintegration of the Larsen B ice shelf, Antarctic Peninsula. *Annals of Glaciology*, *39*, 505–510. https://doi.org/10.3189/172756404781814005Rebesco, M., Domack, E., Zgur, F., Lavoie, C., Leventer, A., Brachfeld, S., Willmott, V., Halverson, G., Truffer, M., Scambos, T., Smith, J., & Pettit, E. (2014). Boundary condition of grounding lines prior to collapse, Larsen-B Ice Shelf, Antarctica. *Science*, *345*(6202), 1354–1358. https://doi.org/10.1126/science.1256697Robel, A. A. (2017). Thinning sea ice weakens buttressing force of iceberg mélange and promotes calving. *Nature Communications*, *8*(1), 14596. https://doi.org/10.1038/ncomms14596Scambos, T. A., Berthier, E., & Shuman, C. A. (2011). The triggering of subglacial lake drainage during rapid glacier drawdown: Crane Glacier, Antarctic Peninsula. *Annals of Glaciology*, *52*(59), 74–82. https://doi.org/10.3189/172756411799096204Scambos, T. A., Bohlander, J. A., Shuman, C. A., & Skvarca, P. (2004). Glacier acceleration and thinning after ice shelf collapse in the Larsen B embayment, Antarctica. *Geophysical Research Letters*, *31*(18). https://doi.org/10.1029/2004GL020670Schlemm, T., & Levermann, A. (2021). A simple parametrization of mélange buttressing for calving glaciers. *The Cryosphere*, *15*(2), 531–545. https://doi.org/10.5194/tc-15-531-2021Studinger, M. (2014). *IceBridge ATM L2 Icessn Elevation, Slope, and Roughness, Version 2.* NASA National Snow and Ice Data Center Distributed Active Archive Center. https://doi.org/10.5067/CPRXXK3F39RVThomas, R., & Studinger, M. (2010). *Pre-IceBridge ATM L2 Icessn Elevation, Slope, and Roughness, Version 1.* NASA National Snow and Ice Data Center Distributed Active Archive Center. https://doi.org/10.5067/6C6WA3R918HJUltee, L., & Bassis, J. (2016). The future is Nye: An extension of the perfect plastic approximation to tidewater glaciers. *Journal of Glaciology*, *62*(236), 1143–1152. https://doi.org/10.1017/jog.2016.108Weertman, J. (1974). Stability of the Junction of an Ice Sheet and an ice Shelf. *Journal of Glaciology*, *13*(67).Wise, M. G., Dowdeswell, J. A., Jakobsson, M., & Larter, R. D. (2016). Evidence of marine ice-cliff instability in Pine Island Bay from iceberg-keel plough marks. *Nature*, *550*, 506–510. https://doi.org/10.1038/nature24458Wuite, J., Rott, H., Hetzenecker, M., Floricioiu, D., De Rydt, J., Gudmundsson, G. H., Nagler, T., & Kern, M. (2015). Evolution of surface velocities and ice discharge of Larsen B outlet glaciers from 1995 to 2013. *The Cryosphere*, *9*(3), 957–969. https://doi.org/10.5194/tc-9-957-2015Xian, X., Chu, M. L., Scavuzzo, R. J., & Srivatsan, T. S. (1989). An experimental evaluation of the tensile strength of impact ice. *Journal of Materials Science Letters*, *8*(10), 1205–1208. https://doi.org/10.1007/BF01730071